J. Cent. South Univ. (2021) 28: 2307−2319
DOI: https://doi.org/10.1007/s11771-021-4771-1

Springer

Quantitative analysis on microstructure and high temperature fracture mechanism of 2.6vol%TiBw/Ti6Al4V composites with equiaxed microstructure after heat treatment

PAN Jin-qi(潘金启), ZHANG Wen-cong(张文丛), YANG Jian-lei(杨建雷),
CHEN Wen-zhen(陈文振), CUI Guo-rong(崔国荣)

School of Materials Science and Engineering, Harbin Institute of Technology (Weihai)
Weihai 264209, China

Abstract: In this paper, the 2.6vol%TiBw/Ti6Al4V composites with network architecture were fabricated by hot press sintering (HPS) at 1100 °C for 1 h, and the quantitative relationships between phases and heat treatment temperatures were established. The results showed that the volume fraction phases changed linearly with a range of solution temperature (930−1010 °C) and aging temperature (400−600 °C). Moreover, the composites with equiaxed microstructure were obtained due to the static recrystallization after solution treated at 950 °C for 1 h and aging treated at 600 °C for 12 h. The ultimate high temperature tensile strengths were 772, 658, 392 and 182 MPa, and the elongations were 9.1%, 12.5%, 28.6% and 35.3% at 400, 500, 600 and 700 °C, respectively. In addition, fractured morphology analysis indicated the excellent strengthening effect of TiBw at a temperature below 600 °C. However, the strengthening effect was significantly reduced due to the debonding of matrix and TiBw at 700 °C and caused the cracks to propagate along the grain boundary.

Key words: titanium matrix composites (TMCs); heat treatment; mechanical properties; microstructure evolution

Cite this article as: PAN Jin-qi, ZHANG Wen-cong, YANG Jian-lei, CHEN Wen-zhen, CUI Guo-rong. Quantitative analysis on microstructure and high temperature fracture mechanism of 2.6vol%TiBw/Ti6Al4V composites with equiaxed microstructure after heat treatment [J]. Journal of Central South University, 2021, 28(8): 2307−2319. DOI: https://doi.org/10.1007/s11771-021-4771-1.

1 Introduction

Due to the good combination of excellent mechanical properties and high temperature durability, titanium matrix composites (TMCs) have attracted more and more attention in the field of military, aerospace and automotive [1−5]. Furthermore, discontinuously reinforced titanium matrix composites (DRTMCs) exhibit significant improvement in various properties, fabricated by in situ methods which TiBw (TiB whisker) and TiCp (TiC particle) have been identified as the best kind of reinforcements owing to their better matrix/reinforcements interfaces and lower cost [6−9]. However, DRTMCs with reinforcement uniformly distributed are easy to introduce impurities, such as oxygen, which are absorbed easily by Ti matrix and can result in deteriorated mechanical properties. Unfortunately, this might restrict the application and development of DRTMCs due to the softened matrix which determines the behavior of the composites. The design proposal of the composites with a network reinforcement distribution by

Foundation item: Project(51905123) supported by the National Natural Science Foundation of China; Project(ZR2019MEM037) supported by the Natural Science Foundation of Shandong Province, China
Received date: 2020-08-22; **Accepted date:** 2020-11-17
Corresponding author: YANG Jian-lei, PhD, Professor; Tel: +86-18660337848; E-mail: jlyang@hit.edu.cn; ORCID: https://orcid.org/0000-0001-9339-2231

HUANG et al [10] solved these problems because the network structure can improve the properties by assembling metals with reinforcement in a controlled way compared with conventional homogeneous TMCs. In addition, DRTMCs with network distributed have been the most probability of being used as structural materials due to their superior properties and good durability at room and high temperature [7, 11−13]. Powder metallurgy (PM) such as hot press sintering (HPS) has been considered as an effective method to fabricate DRTMCs with network microstructure compared with conventional PM technique which exhibited extreme brittleness and low ductility [10, 11, 14].

To further improve the strength and ductility of DRTMCs at room and high temperature, researchers have done lots of studies on the strengthening of DRTMCs by thermal processing and subsequent heat treatment [15−18]. ZHANG et al [17] pointed out that TiBw/TA15 composites could be strengthened after heat treatment that ultimate tensile strength improved 200 MPa and elongation also increased to 9.9% at 600 °C. Furthermore, QI et al [19] fabricated TiC/TA15 composites by induction melting. High temperature tensile results revealed that heat treatment could significantly enhance tensile strength and the temperature had a great influence on high temperature performance. ZHANG et al [20] fabricated TiBw/Ti6Al4V by pre-sintering and canned powder extrusion followed by the treatment of water quenching at 1000 °C and aging at 600 °C, and found that the fraction of martensite α' increased with the rising solution temperature, which resulted in a significant improvement not only in strength but also in elongation at ambient and high temperature. These studies revealed the fact that heat treatment could change the microstructure morphology which improved the properties of DRTMCs. However, the quantitative relationship between the heat treatment parameters and the volume fraction of microstructure in DRTMCs has seldom been put forward. Therefore, adjusting the microstructure morphology is very important to obtain DRTMCs with superior mechanical properties.

In this work, the 2.6vol%TiBw/Ti6Al4V composites were fabricated by HPS with subsequent heat treatment of different parameters to obtain different microstructure morphology. The quantitative relationships between the heat treatment parameters and microstructure were set up. The equiaxed microstructure composites were obtained and the formation mechanism of this kind of microstructure was discussed. In addition, the mechanical properties at room temperature and high temperature were tested and the fracture mechanism at high temperature was investigated.

2 Materials and experimental procedures

The materials used in this work were Ti6Al4V (100−150 μm) powders and TiB_2 powders, supplied by Shanxi Yuguang Phelly Metal Materials Co. Itd., China. First, the two kinds of powders were put into a planetary ball mill machine at a speed of 100 r/min for 6 h under a protective atmosphere of argon and the weight ratio of balls to powders was 5:1 in order to make TiB_2 powders adhere onto the surface of Ti6Al4V particles homogeneously. Next, the blended powders were sintered at 1100 °C for 1 h under the pressure of 25 MPa. TiB whiskers giving about 2.6 vol% were synthesized in situ reaction $Ti+TiB_2 \rightarrow 2TiB$ during the sintering process [7, 21]. It is worth noting that a larger content of reinforcement (>5 vol%) would greatly reduce the plasticity of the material, so we chose a moderate ratio with better strength and toughness. Finally, a cylindrical billet was sintered and the size was Φ30 mm×70 mm. The preparation of 2.6vol%TiBw/Ti6Al4V composites was shown in Figure 1.

In order to further investigate the quantitative relationship of heat treatment on the microstructure of TiBw/Ti6Al4V composites with network architecture, the specimens were solution-treated between 930 and 1100 °C with an interval of 20 °C for 1 h followed by subsequent aging temperature at the range of 400 to 600 °C with an interval of 50 °C for 6 h and 12 h. The solution specimens were cooled by water quenching (WQ) and the aging specimens were directly air-cooled (AC). The images were captured by scanning electron micrograph (SEM) and the volume fractions were measured using Image Pro Plus software. The composites with equiaxed microstructure were obtained by heat treatment and the evolution of this microstructure was investigated with electron back-scattered diffraction (EBSD).

The specimens for tensile tests and microstructural observation were cut from the billet

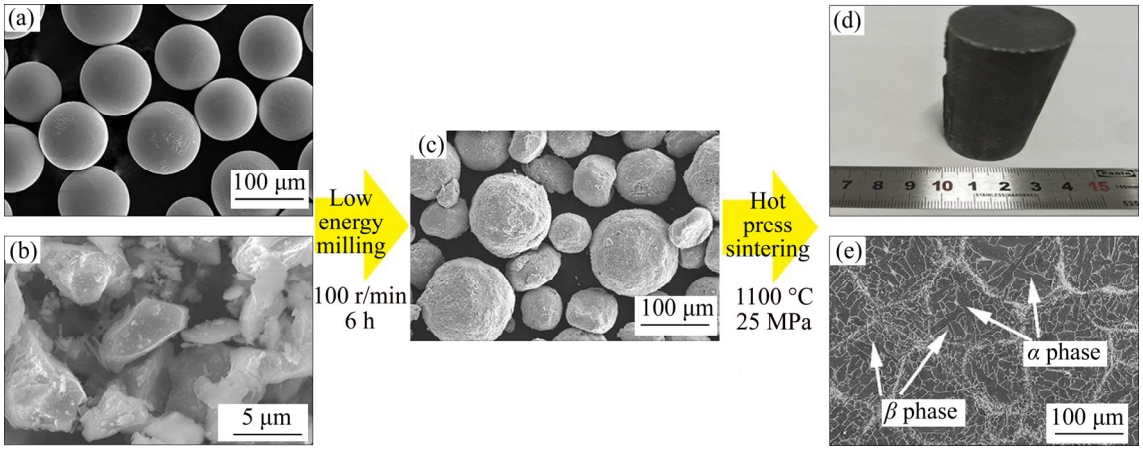

Figure 1 Preparation of 2.6vol%TiBw/Ti6Al4V composites: (a) Original Ti6Al4V powders; (b) TiB_2 powders; (c) Mixed powders; (d) Sintered cylindrical billet; (e) SEM of sintered composites

using an electric spark cutting machine and the gauge dimensions of the tensile specimens were 15 mm×4 mm×1.5 mm. Before the experiments, the samples were polished using metallographic sandpaper and then the samples of microstructural observation were etched in Kroll's solution (5 vol% HF+10 vol% HNO_3+85 vol% H_2O) for 8 to 10 s. The phase identification was made by X-ray diffraction (XRD) using XD-2700 equipment. The tensile tests were carried out using Instron-5500R at different temperatures (room temperature, 400, 500, 600 and 700 °C) with the speed of 0.5 mm/min and each test was repeated at least three times. Meanwhile, the fracturing and strengthening mechanism was analyzed in detailed.

3 Results

3.1 Phase identification

Figure 2 shows the X-ray diffraction (XRD) pattern of the original Ti6Al4V powders and the mixed powders after ball milling for 6 h, only Ti and TiB_2 exist in the mixed powders and no TiB phase is detected. The results indicate that there is no chemical reaction between TiB_2 and Ti6Al4V matrix, but only TiB_2 powders adhere around the Ti6Al4V particles during the ball milling. The aim of low-energy milling instead of high-energy milling is to adhere fine TiB_2 particles onto the surface of large Ti particles and they only occur physical coupling. In addition, low-energy milling can not only guarantee the reinforcement network distribution, but also protect the Ti matrix from absorbing oxygen (O) and hydrogen (H). However,

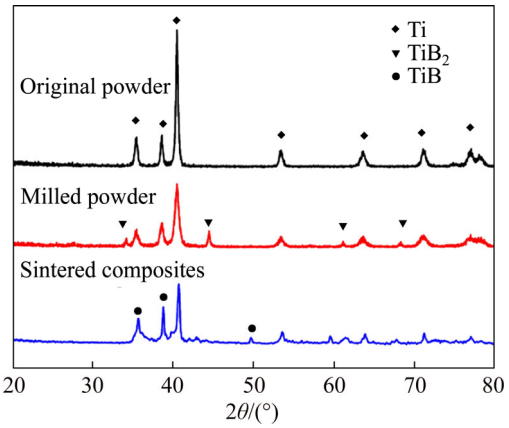

Figure 2 XRD pattern of mixed powders and sintered composites

the TiB phase is exhibited in the sintered composites and no residual TiB_2 phase is detected. It means that the TiB was in situ synthesized from Ti and TiB_2 powders during the HPS process, because the in situ reaction can proceed spontaneously at 1100 °C. Moreover, the growth of TiB is controlled by diffusion of B and Ti elements in TiB and TiB exhibits a one-dimensional growth pattern and eventually forms a whisker-like morphology due to the fastest diffusion rate of B element in TiB [22]. The interface between matrix and TiBw is clean and no other impurities are produced during the in-situ synthesis process as shown in Figure 1(e).

3.2 Microstructure

Figure 3 shows the SEM micrographs of the sintered 2.6vol%TiBw/Ti6Al4V composites after solution treated from 950 to 1100 °C for 1 h. The matrix is composed of martensite α' phase, primary

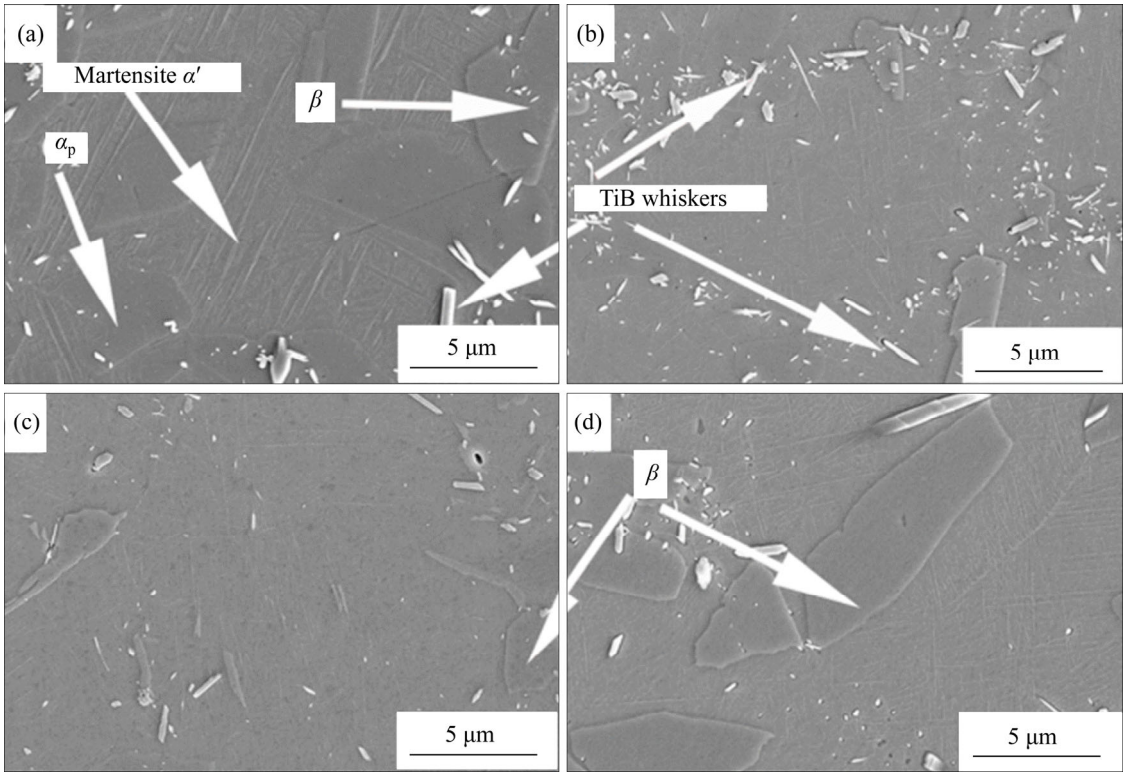

Figure 3 Microstructure of composites after solution treated at different temperatures for 1 h: (a) 950 °C; (b) 1000 °C; (c) 1050 °C; (d) 1100 °C

α phase (α_p) and residual high temperature β phase which nucleated at the grain boundaries and did not convert into α' during the rapid cooling process as shown in Figure 3(a). Compared with Figure 1(e), the Widmanstatten $\alpha+\beta$ phase transforms to martensite α' phase and high temperature β phase after quenching at 950 °C. The increase in solution temperature promotes the transformation of α_p phase to α' phase and β phase as shown in Figures 3(b)−(d). And the quantitative results of solution temperature and the volume fraction of α' ($V_{\alpha'}$), α_p (V_{α_p}) and residual β (V_β) are shown in Table 1. Figure 4 depicts $V_{\alpha'}$, $V\alpha_p$ and V_β with different solution temperatures (T_s). As the T_s increases from 930 to 1010 °C, the V_{α_p}, $V_{\alpha'}$ and V_β fit the linear changes (V_{α_p}=402.11−0.398T_s, $V_{\alpha'}$=−283.66+0.353T_s, V_β=−21.2+0.045T_s). But when the T_s increases to 1050 °C, they do not fit these rules due to the dynamic balance of the phase transition. It is worth noting that the content of TiBw (V_{TiB_w}) is almost staying the same as shown in Table 1.

Table 1 shows V_{α_p} and $V_{\alpha+\beta}$ versus the solution and aging temperatures. The curves reveal the fact that the volume fraction of fine $\alpha+\beta$ phase, which was disintegrated from martensite α' during the aging process, nearly fitting the linear changes versus solution temperature (930−1010 °C) with aging for 6 h at 400, 450, 500 and 550 °C, respectively, as shown in Figure 5. The expression are listed as follows:

$$V_{\alpha_p}=273.875-0.2235T_s \text{ (400 °C)} \quad (1)$$

$$V_{\alpha_p}=271.51-0.223T_s \text{ (450 °C)} \quad (2)$$

$$V_{\alpha_p}=272.38-0.226T_s \text{ (500 °C)} \quad (3)$$

$$V_{\alpha_p}=256.48-0.212T_s \text{ (550 °C)} \quad (4)$$

$$V_{\alpha_p}=273.865-0.2325T_s \text{ (600 °C)} \quad (5)$$

In addition, the $V_{\alpha+\beta}$ could be calculated by $V_{\alpha+\beta}=1-V_{\alpha_p}-V_{TiBw}$, because the composites were composed by α_p phase, fine $\alpha+\beta$ phase and TiB whiskers. According to Eq. (1) to Eq. (5), it can be seen that V_{α_p} exhibits an inverse relation with solution and aging temperature, which means that the volume fraction of α_p decreases with the increasing solution and aging temperature. Therefore, the relationship between the volume of primary α phase (V_{α_p}), $\alpha+\beta$ phase ($V_{\alpha+\beta}$) and solution temperature (T_s), aging temperature (T_a) can be concluded as:

$$V_{\alpha_p}= 291.4621-0.2234T_s-0.04368T_a \quad (6)$$

$$V_{\alpha+\beta}=1-V_{\alpha_p}-V_{TiBw} \quad (7)$$

Table 1 Volume fraction of different phase after solution and aging treatment

T_s (1 h)/°C	T_a(6 h)/°C	V_{α_p}/%	$V_{\alpha+\beta}$/%
930	400	66.1±4.5	31.2±1.2
930	450	64.7±5.6	32.5±2.3
930	500	62.5±3.4	34.9±3.2
930	550	59.5±3.8	37.8±2.5
930	600	57.1±2.8	40.1±2.4
950	400	61.8±3.9	35.6±1.8
950	450	59.1±5.2	38.2±2.2
950	500	57.7±4.5	39.7±1.4
950	550	55.4±4.1	42.0±2.4
950	600	54.0±3.1	43.5±1.1
970	400	56.4±2.6	41.0±3.4
970	450	55.0±3.4	42.2±3.1
970	500	52.5±3.6	44.9±1.4
970	550	50.3±2.6	46.9±2.8
970	600	48.3±1.9	48.8±3.3
990	400	52.9±2.1	44.5±3.7
990	450	50.5±1.6	46.8±4.2
990	500	48.7±2.9	48.7±3.8
990	550	46.0±2.4	51.3±2.8
990	600	42.9±3.0	54.5±3.4
1010	400	48.2±2.1	49.0±2.8
1010	450	46.7±3.8	50.7±3.9
1010	500	44.4±2.0	53.0±2.7
1010	550	43.0±2.6	54.4±1.7
1010	600	39.4±1.7	57.7±2.1

To obtain different microstructure morphologies of 2.6vol%TiBw/Ti6Al4V composites, the target temperature and time were changed during the heat treatment. Figure 6 shows the microstructure of the composites with different heat treatment parameters and the matrix exhibits an equiaxed microstructure after solution at 950 °C for 1 h and aging at 600 °C for 12 h. Comparing Figure 3 with Figure 6, the acicular martensite α' phase and residual β phase transform into fine $\alpha+\beta$ phase after aging for 12 h and the lath α_p in the matrix gradually spheroidizes, forming equiaxed α phase (10−20 μm) as the aging temperature increases to 600 °C [16, 23]. This phenomenon indicates that increasing the aging temperature could inspire the aggregation of α phase effectively due to the sufficient spheroidization time. However, as the aging temperature increases to 700 °C, the

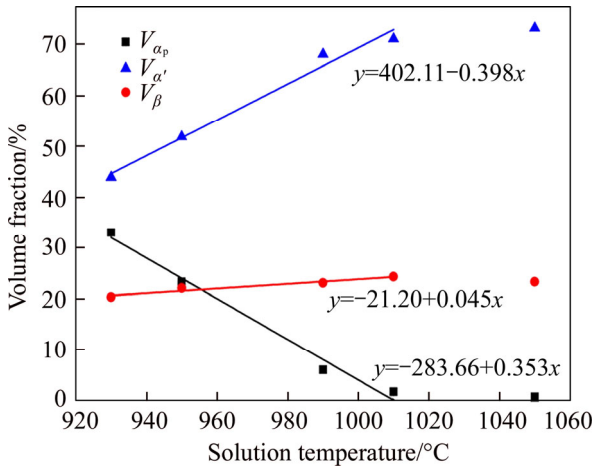

Figure 4 V_{α_p}, $V_{\alpha'}$ and V_β versus solution temperature for 2.6vol%TiBw/Ti6Al4V composites

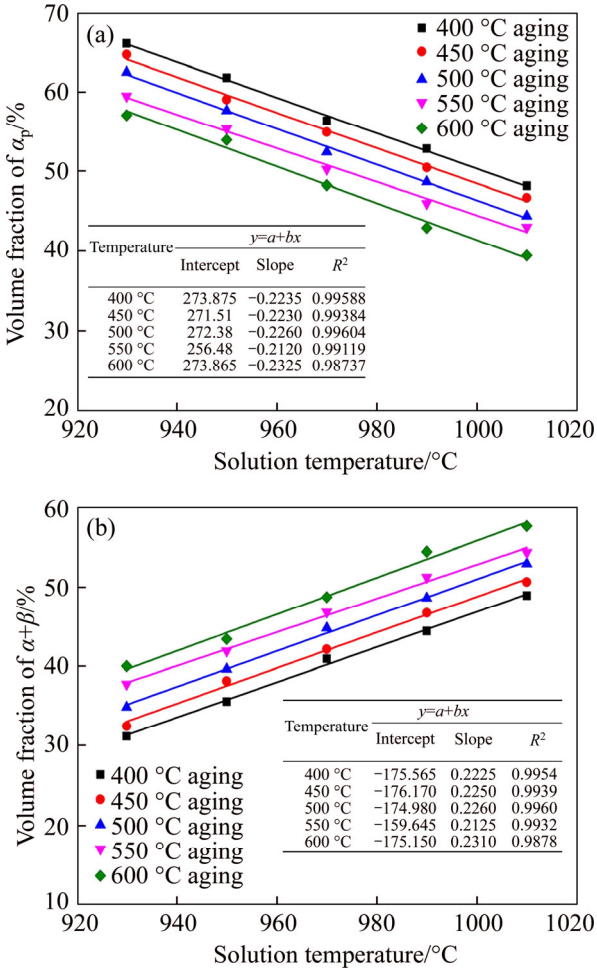

Figure 5 Relationships between volume fraction of phases and temperature of solution and aging: (a) V_{α_p}; (b) $V_{\alpha+\beta}$

matrix consists of coarse $\alpha+\beta$ phase and few α phases which stay at the boundary of the grains.

Figure 7 shows the kernel average misorientation (KAM) and misorientation angle

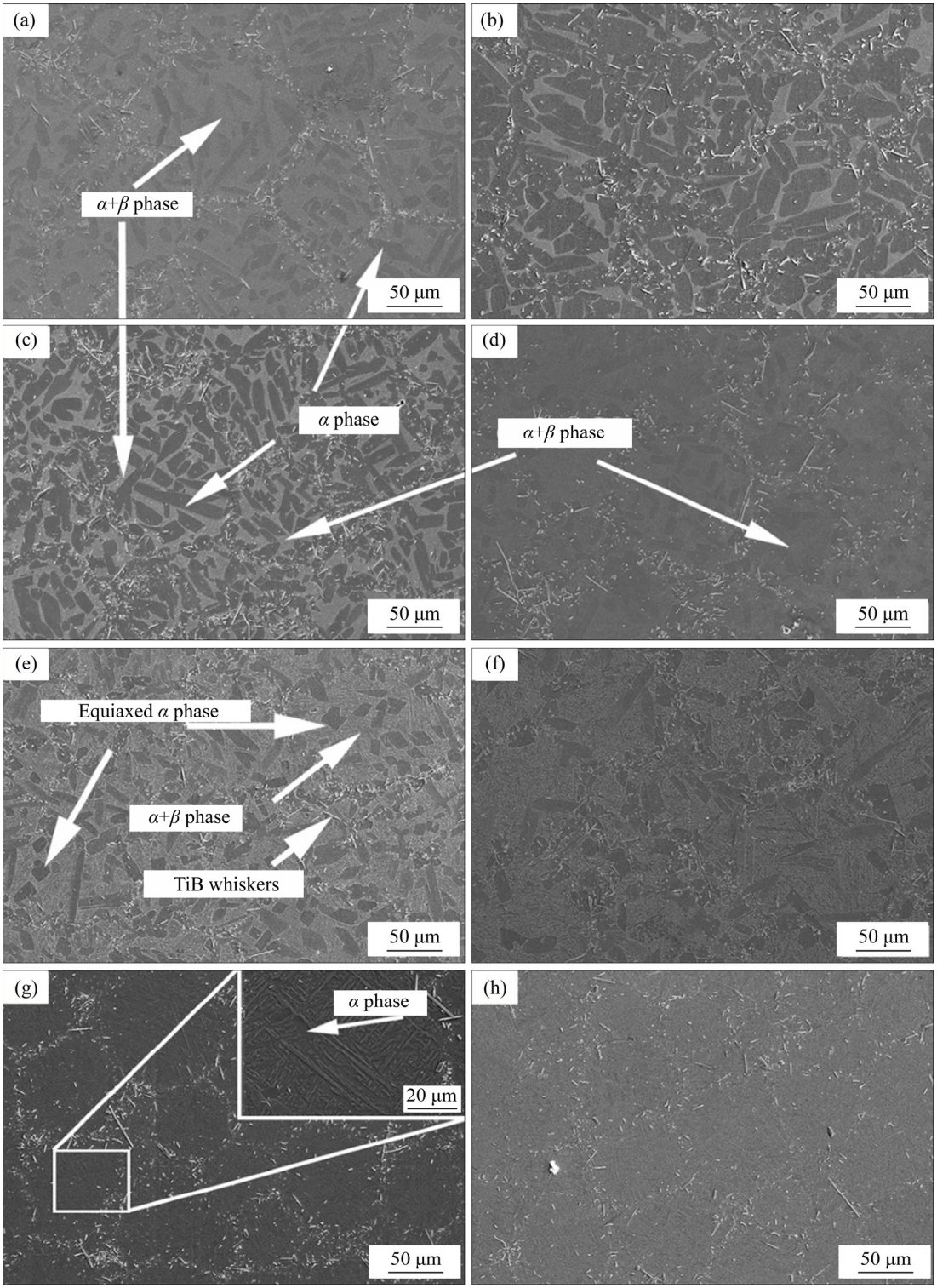

Figure 6 SEM of 2.6vol%TiBw/Ti6Al4V composites (a) T_s=950 °C, T_a=400 °C; (b) T_s=1050 °C, T_a=400 °C; (c) T_s=950 °C, T_a=500 °C; (d) T_s=1050 °C, T_a=500 °C; (e) T_s=950 °C, T_a=600 °C; (f) T_s=1050 °C, T_a=600 °C; (g) T_s=950 °C, T_a=700 °C; (h) T_s=1050 °C, T_a=700 °C

(MA) of the equiaxed microstructure and the sintered microstructure of the composites. Comparing Figure 7(a) with Figure 7(b), most of the plastic deformation of the powders in the sintered composites are eliminated after heat treatment. However, there is still a little residual strain existing at the grain boundaries. Moreover, the volume fraction of low angle grain boundary (LAGB) in the sintered composites is higher than the composites with equiaxed microstructure as

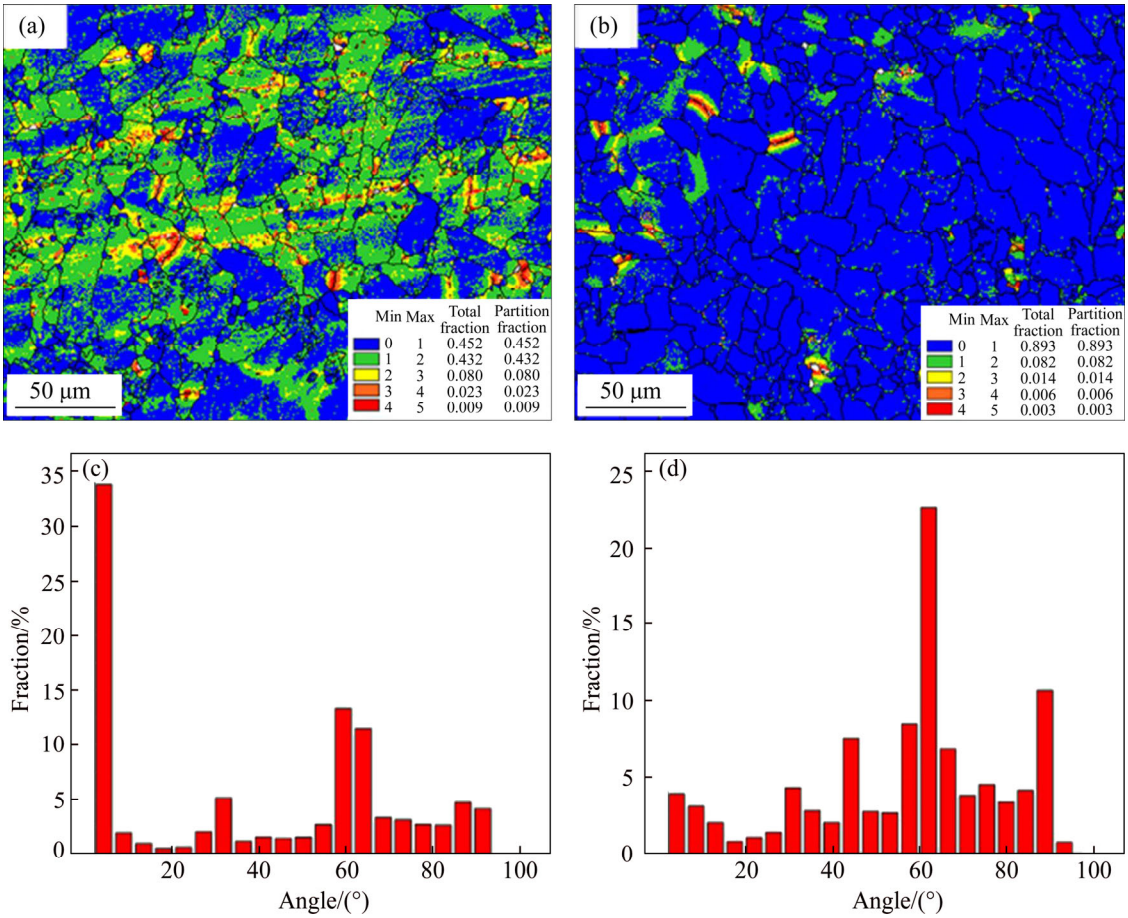

Figure 7 (a) KAM of sintered microstructure; (b) KAM of equiaxed microstructure; (c) MA of sintered microstructure; (d) MA of equiaxed microstructure

shown in Figures 7(c) and (d). The misorientation angle peaks of the sintered microstructure concentrate around 5° and 60° while the equiaxed microstructure concentrate around 45°, 60° and 90°.

3.3 Mechanical properties

Figure 8 shows the room temperature and high temperatures tensile stress−strain curves of the 2.6vol.%TiBw/Ti6Al4V composites with equiaxed microstructure. Compared with the sintered composites, the room temperature strength of equiaxed microstructure increases from 810 to 998 MPa and the elongation increases from 4.9% to 7.6%. The results show that compared with the sintered composites, the strength and plasticity of the composites with equiaxed microstructure are significantly improved. At high temperature, the tensile strength of the composites decreases to 772 MPa (at 400 °C) and 658 MPa (at 500 °C), respectively. However, the strength sharply decreases to 392 and 182 MPa when the test

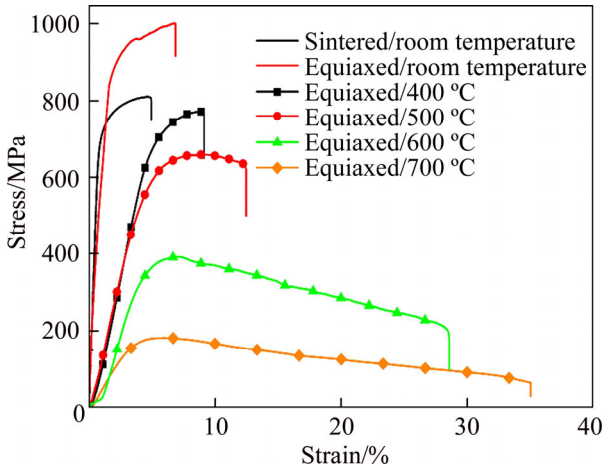

Figure 8 Tensile properties of 2.6vol%TiBw/Ti6Al4V composites with equiaxed microstructure at different temperatures

temperature increases to 600 and 700 °C. On the contrary, the elongation of the composites continuously increases from 9.1% at 400 °C to 35.3% as the test temperature is elevated to 700 °C.

Figure 9 shows the micrographs of the fracture

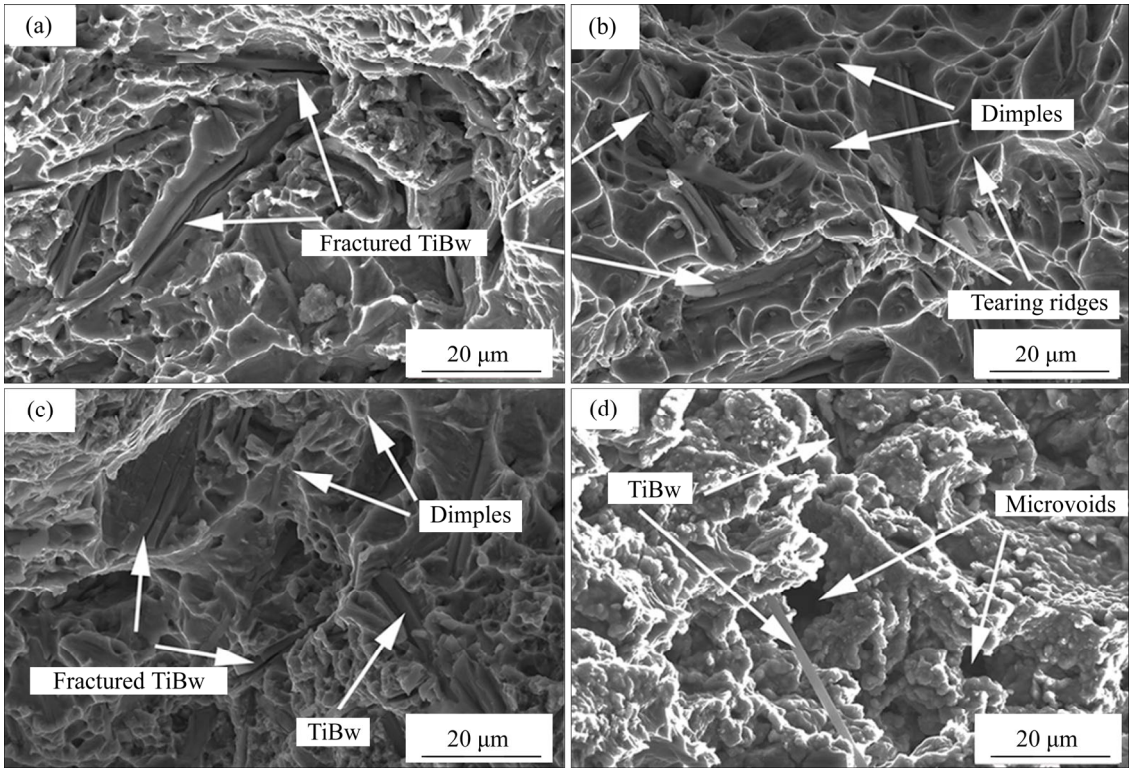

Figure 9 Fracture morphology of equiaxed microstructure at different testing temperature: (a) 400 °C; (b) 500 °C; (c) 600 °C; (d) 700 °C

surfaces of the equiaxed microstructure composites at 400, 500, 600 and 700 °C, respectively. As shown in Figure 9(a), the fractured TiBw, tearing ridges and some shallow dimples in the matrix which are beneficial to the elongation of the composites can be observed. With the test temperature increasing, the dimples become more and deeper. However, when the test temperature increases to 700 °C, the fractured TiBw can hardly be discovered but some microvoids appear.

In order to further investigate the fracture process of the TiBw/Ti6Al4V composites at high temperature, the SEM micrographs of the fractured samples from the longitudinal direction were shown in Figure 10. From Figures 10(a) and (b), many multiple fractured TiBw can be seen at the grain boundary and the micropores are exhibited around the fractured TiBw when the test temperature is below 500 °C. With increasing the test temperature, the matrix begins softening and the micropores coalescence around the TiBw as shown in Figure 10(c). When the test temperature increases to 700 °C, the debonding of matrix and TiBw becomes severe and there are many cracks at the grain boundary in Figure 10(d).

4 Discussion

4.1 Evolution of equiaxed microstructure

From Figure 1(e), it can be seen that the matrix is Widmanstatten which consists of lamellar α phase (the black area) and β (the white area) phase with the TiB whiskers surrounded at the boundary of the grains. When sintered at 1100 °C, above the β phase transition temperature (995 °C), the α phase is completely converted into high temperature β phase and then new α phases nucleate at the high temperature β grain boundary and grow inside the grain to form α clusters with residual β alternately distributed in the subsequent cooling process [24]. After solution treated at 950 °C for 1 h, most of the Widmanstatten α+β phases transform into martensite α' phase and high temperature β phase while some retain as primary α phase as shown in Figure 3. In addition, the volume fractions of α' and β increase with increasing the solution temperature from 930 to 1100 °C which can improve the strength but decline the ductility as shown in Figure 4.

After aging at 600 °C for 12 h, equiaxed α phase and fine α+β phase microstructure

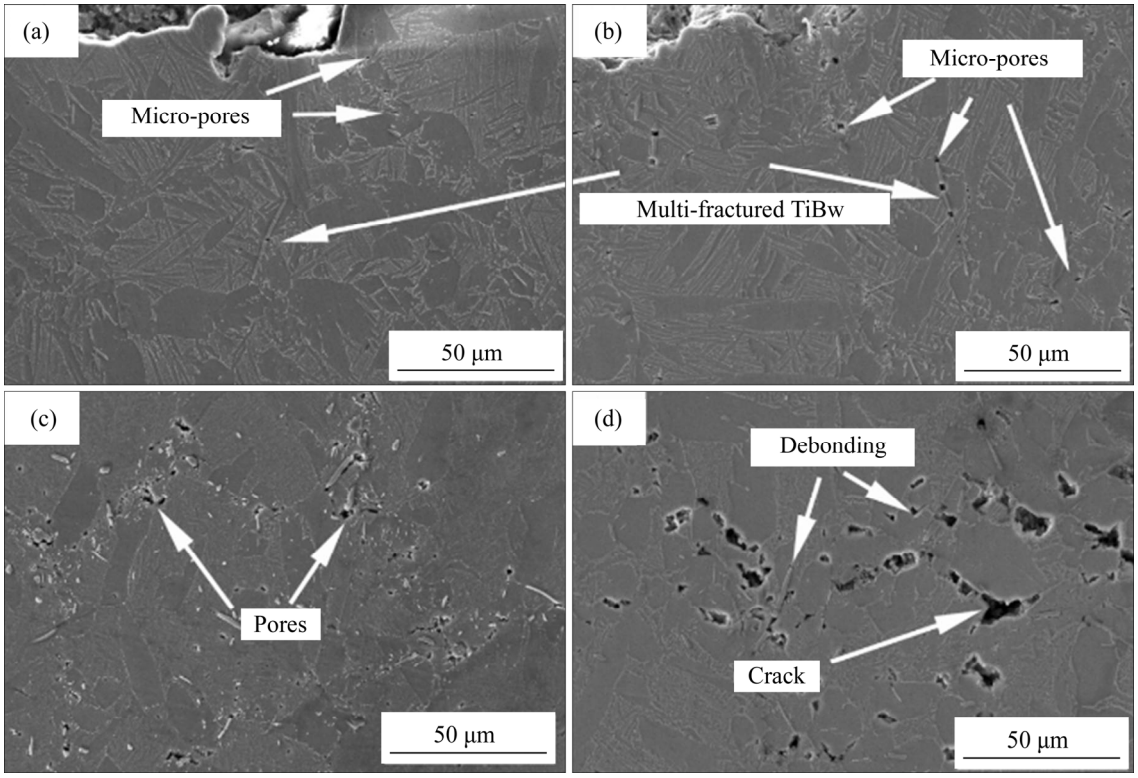

Figure 10 SEM of fractured samples from longitudinal direction at different temperature: (a) 400 °C; (b) 500 °C; (c) 600 °C; (d) 700 °C

transformed from the martensite α' phase as shown in Figure 6(e). This equiaxed microstructure exhibits higher strength and ductility than Widmanstatten. It is worth noting that both the size and content of the fine $\alpha+\beta$ phase increase with the aging temperature increases to 700 °C, which is harmful to the strength of the composites [23].

Figure 7 shows the variation in KAM and MA of the equiaxed microstructure composites in order to further explain the evolution during the heat treatment process. The results indicate that the residual strain produced during hot press sintering at 1100 °C decreased and the static recrystallization occurred during heat treatment. Because of the orientation relationship between the phases and the semi-coherent nature of the boundaries, the energy of the interfaces is low [25]. However, the initial semi-coherent boundary can be transformed into a high-energy incoherent boundary by heat treatment and the spheroidization of α phase was enhanced as the aging time extends to 12 h. It is meaningful to point out that the actual peaks of MA concentrate around 45°, 60° and 90°, indicating that the formation of equiaxed α phase from martensite α' phase during the aging process fitting the Burgers relationship [26].

4.2 High temperature fracture mechainsm

The stress−strain curves of the equiaxed microstructure are significantly affected by the testing temperature as shown in Figure 8. Increasing the test temperature from 400 to 700 °C, the peak stress tends to decrease. It is obvious that the curves can be divided into four parts: the work-hardening stage, the flow-softening stage, the steady-state stage and the fractured stage [27, 28]. The decrease of the strength can be attributed to the TiBw fracturing and the matrix softening with the test temperature increasing as shown in Figure 9. Moreover, high temperature oxidation also has a great influence on the performance of the composites. From Figures 9(a)−(c), there is no obvious trace of oxidation near the fracture due to the excellent oxidation resistance below 600 °C. However, as the temperature increases to 700 °C, the fracture morphology exhibits gel-like, the dimples and tearing edges are completely indistinguishable. This phenomenon could be attributed to high temperature oxidation which greatly reduces the strength of the composites by forming oxidation films.

The fracture morphology of the composites with equiaxed microstructure at different

temperatures can be concluded as follows: From a micro perspective, as the stress is applied, the TiBw bear the stress until the stress is beyond the bearing capability because the TiBw can bear higher stress than the soft matrix at 400, 500 and 600 °C. The migration of dislocation is promoted during the plastic deformation and is hindered at TiBw. The pile up of the dislocation caused by the stress concentration leads to the TiBw prior bear stress and fracture due to the high contiguity of reinforcement in the composites with network microstructure. Because of the micropores can be blunted by the matrix, the fractured TiBw can continuous bear load until multiple fractures occurs in the TiBw, as shown in Figures 10(a)−(c), indicating that the combination of whiskers and matrix is good and the TiBw can play an important role in strengthening the composites at 600 °C. However, the strengthening effect is significantly reduced due to the debonding of matrix and TiBw at 700 °C.

In order to better understand the tensile fracture mechanism of the composites with equiaxed microstructure at high temperature (700 °C), the fracture process can be concluded as shown in Figure 11. The fractured samples can be divided into four different parts according to the distance from the fractured surface referring to the in situ tensile process [29]: elastic deformation area (Area A), small deformation area (Area B), severe deformation area and fracture area (Area C). In the elastic deformation stage, there are no microvoids and fractured TiBw in the matrix and the matrix exhibits the equiaxed microstructure in Figures 11(b) and (f). Some well-bonded whiskers could still play an enhanced role in the composites. With the stress increasing, the reinforcement particles fractured prior to the ductile matrix but the TiBw could

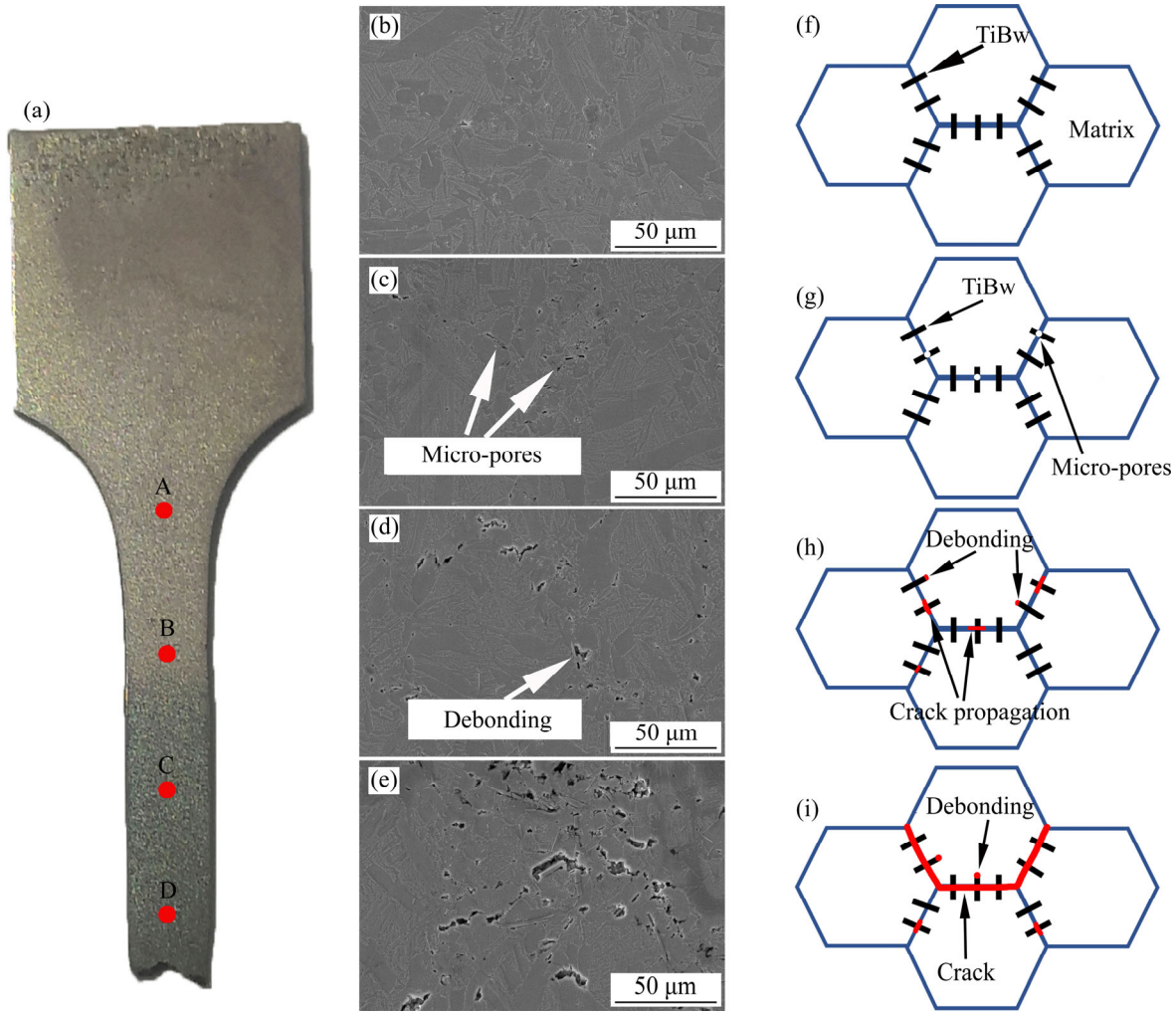

Figure 11 Tensile fracture mechanisms of 2.6vol%TiBw/Ti6Al4V composites with equiaxed microstructure at 700 °C: (a) Fractured sample; (b, f) Undeformed area; (c, g) Small deformation area; (d, h) Severe deformation area; (e, i) Fracture area

hardly multiple fracture due to the decreasing combination at high temperature. In the small deformation stage, the debonding of the matrix and TiBw begins occurring. Moreover, the micropores are exhibited at the fractured TiBw and the debonding place under the outer stress as shown in Figures 11(c) and (g). As the deformation continues, the debonding becomes severe and the micropores keep gathering to form pores around TiBw at the grain boundary, resulting in the propagation of microcracks along the grain boundary as shown in Figures 11(d) and (h). Finally, in the fractured stage, the crack is formed which leads to the fracture of the composites as shown in Figures 11(e) and (i). The fracture mechanism of the composites indicates that the strengthening effect of TiBw is significantly reduced at a temperature above 700 °C.

5 Conclusions

In this study, the network 2.6vol%TiBw/Ti6Al4V composites with equiaxed microstructure were successfully fabricated by HPS and heat treatment. Moreover, the quantitative relationships between the heat treatment parameters and microstructure were established. In addition, tensile tests of the composites were carried out at room temperature, 400, 500, 600 and 700 °C, respectively. The main conclusions of this work can be summarized as follows:

1) The volume fraction of β phase and α' phase increases while the volume fraction of α_p phase decreases fitting the linear changes with increasing the solution temperature from 930 to 1100 °C. And the volume fraction of α_p phase and fine $\alpha+\beta$ phase also fit linear changes with solution temperature and aging temperature.

2) The spheroidization occurs in the microstructure and the equiaxed microstructure is formed after solution at 950 °C for 1 h and aging at 600 °C for 12 h.

3) The tensile strength and elongation of the composites with equiaxed microstructure by the heat treatment of 950 °C/1 h/WQ and 600 °C/12 h/AC are increased by 23.2% and 55.1% comparing with the sintered composites. The high temperature tensile strength at 400, 500, 600 and 700 °C can be 772, 658, 392 and 182 MPa, respectively.

4) The TiBw can bear the stress until multiple fractures occur in the TiBw when the temperature is below 600 °C due to a good combination of whiskers and matrix. However, the strengthening effect of TiBw is significantly reduced due to the debonding of matrix and TiBw at 700 °C and causing the cracks to propagate along the grain boundary.

Contributors

The overarching research goals were developed by ZHANG Wen-cong, YANG Jian-lei, CUI Guo-rong and CHEN Wen-zhen. PAN Jin-qi and ZHANG Wen-cong conducted the experiments and analyzed the measured data. PAN Jin-qi and YANG Jian-lei wrote the initial draft of the manuscript. All authors replied to reviewers' comments and revised the final version.

Conflict of interest

PAN Jin-qi, ZHANG Wen-cong, YANG Jian-lei, CHEN Wen-zhen, and CUI Guo-rong declare that they have no conflict of interest.

References

[1] BROZEK C, SUN F, VERMAUT P, MILLET Y, LENAIN A, EMBURY D, JACQUES P J, PRIMA F. A β-titanium alloy with extra high strain-hardening rate: Design and mechanical properties [J]. Scripta Materialia, 2016, 114: 60−64. DOI: 10.1016/j.scriptamat.2015.11.020.

[2] HUANG L J, GENG L, PENG H X. Microstructurally inhomogeneous composites: Is a homogeneous reinforcement distribution optimal? [J]. Progress in Materials Science, 2015, 71: 93−168. DOI: 10.1016/j.pmatsci.2015.01.002.

[3] HUANG B, YANG Y, LUO H, YUAN M. Effects of the coating system and interfacial region thickness on the thermal residual stresses in SiCf/Ti–6Al–4V composites [J]. Materials & Design, 2009, 30(3): 718−722. DOI: 10.1016/j.matdes.2008.05.013

[4] WANG J, GUO X, QIN J, ZHANG D, LU W. Microstructure and mechanical properties of investment casted titanium matrix composites with B4C additions [J]. Materials Science and Engineering A, 2015, 628: 366−373. DOI: 10.1016/j.msea.2015.01.067.

[5] LU H, ZHANG D, GABBITAS B, YANG F, MATTHEWS S. Synthesis of a TiBw/Ti6Al4V composite by powder compact extrusion using a blended powder mixture [J]. Journal of Alloys and Compounds, 2014, 606: 262−268. DOI: 10.1016/j.jallcom.2014.03.144.

[6] SELVAKUMAR M, CHANDRASEKAR P, MOHANRAJ M, RAVISANKAR B, BALARAJU J N. Role of powder metallurgical processing and TiB reinforcement on mechanical response of Ti–TiB composites [J]. Materials

Letters, 2015, 144: 58−61. DOI: 10.1016/j.matlet.2014.12.126.

[7] CHEN W, YANG J, ZHANG W, WANG M, DU D, CUI G. Influence of TiBw volume fraction on microstructure and high-temperature properties of in situ TiBw/Ti6Al4V composites with TiBw columnar reinforced structure fabricated by pre-sintering and canned extrusion [J]. Advanced Powder Technology, 2017, 28(9): 2346−2356. DOI: 10.1016/j.apt.2017.06.016.

[8] LU W J, ZHANG D, ZHANG X N, WU R J, SAKATA T, MORI H. Creep rupture life of in situ synthesized (TiB+TiC)/Ti matrix composites [J]. Scripta Mater, 2001, 44: 2449−2455. DOI: 10.1016/S1359-6462(01)00926-5.

[9] HU H T, HUANG L J, GENG L, SUN J F, TIAN H. High temperature mechanical properties of as-extruded TiBw/Ti60 composites with ellipsoid network architecture [J]. Journal of Alloys and Compounds, 2016, 688: 958−966. DOI: 10.1016/j.jallcom.2016.07.118.

[10] HUANG L J, GENG L, LI A B, YANG F Y, PENG H X. In situ TiBw/Ti6Al4V composites with novel reinforcement architecture fabricated by reaction hot pressing [J]. Scripta Materialia, 2009, 60: 996−999. DOI: 10.1016/j.scriptamat.2009.02.032.

[11] MORSI K, PATEL V V. Processing and properties of titanium–titanium boride (TiBw) matrix composites—A review [J]. Journal of Materials Science, 2007, 42(6): 2037−2047. DOI: 10.1007/s10853-006-0776-2.

[12] HUANG L J, GENG L, PENG H X, KAVEENDRAN B. High temperature tensile properties of in situ TiBw/Ti6Al4V composites with a novel network reinforcement architecture [J]. Materials Science and Engineering A, 2012, 534: 688−692. DOI: 10.1016/j.msea.2011.12.028.

[13] WANG B, HUANG L J, GENG L, RONG X D, LIU B X. Effects of heat treatments on microstructure and tensile properties of as-extruded TiBw/near-α Ti composites [J]. Materials & Design, 2015, 85: 679−686. DOI: 10.1016/j.matdes.2015.07.058.

[14] HUANG L J, YANG F Y, HU H T, RONG X D, GENG L, WU L Z. TiB whiskers reinforced high temperature titanium Ti60 alloy composites with novel network microstructure [J]. Materials & Design, 2013, 51: 421−426. DOI: 10.1016/j.matdes.2013.04.048.

[15] HILL D, BANERJEE R, HUBER D, TILEY J, FRASER H L. Formation of equiaxed alpha in TiB reinforced Ti alloy composites [J]. Scripta Materialia, 2005, 52(5): 387−392. DOI: 10.1016/j.scriptamat.2004.10.019.

[16] RASTEGARI H A, ASGARI S, ABBASI S M. Producing Ti–6Al–4V/TiC composite with good ductility by vacuum induction melting furnace and hot rolling process [J]. Materials & Design, 2011, 32(10): 5010−5014. DOI: 10.1016/j.matdes.2011.06.009.

[17] ZHANG R, WANG D J, HUANG L J, YUAN S J. Effects of heat treatment on microstructure and high temperature tensile properties of TiBw/TA15 composite billet with network architecture [J]. Materials Science and Engineering A, 2017, 679: 314−322. DOI: 10.1016/j.msea.2016.10.0.

[18] HUANG L J, XU H Y, WANG B, ZHANG Y Z, GENG L. Effects of heat treatment parameters on the microstructure and mechanical properties of in situ TiBw/Ti6Al4V composite with a network architecture [J]. Materials & Design, 2012, 36: 694−698. DOI: 10.1016/j.matdes.2011.12.021.

[19] QI J Q, WANG H W, ZOU C M, WEI Z J. Influence of matrix characteristics on tensile properties of in situ synthesized TiC/TA15 composite [J]. Materials Science and Engineering A, 2012, 553: 59−66. DOI: 10.1016/j.msea.2012.05.092.

[20] ZHANG W, FENG Y, CHEN W, YANG J. Effects of heat treatment on the microstructure and mechanical properties of in situ inhomogeneous TiBw/Ti6Al4V composite fabricated by pre–sintering and canned powder extrusion [J]. Journal of Alloys and Compounds, 2017, 693: 1116−1123. DOI: 10.1016/j.jallcom.2016.09.229.

[21] LI B S, SHANG J L, GUO J J, FU H Z. Formation of TiBw reinforcement in in-situ titanium matrix composites [J]. J Mater Sci, 2004, 39: 1131−1133.

[22] FAN Z, GUO Z X, CANTOR B. The kinetics and mechanism of interfacial reaction in sigma fibre-reinforced Ti MMCs [J]. Composites Part A−Applied Science and Manufacturing, 1997, 28(2): 131−140. DOI: 10.1016/S1359-835X(96)00105-4.

[23] HUANG L J, GENG L, WANG B, XU H Y, KAVEENDRAN B. Effects of extrusion and heat treatment on the microstructure and tensile properties of in situ TiBw/Ti6Al4V composite with a network architecture [J]. Composites Part A−Applied Science and Manufacturing, 2012, 43(3): 486−491. DOI: 10.1016/j.compositesa.2011.11.014.

[24] JIAO X, CHEN W, YANG J, ZHANG W, WANG G. Microstructure evolution and high-temperature tensile behavior of the powder extruded 2.5 vol%TiBw/TA15 composites [J]. Materials Science and Engineering A, 2019, 745: 353−359. DOI: 10.1016/j.msea.2018.12.095.

[25] SERGEY Z, GENNADY S, S. LEE S. Loss of coherency of the alpha/beta interface boundary in titanium alloys during deformation [J]. Philosophical Magazine Letters, 2010, 90(12): 903−914. DOI: 10.1080/09500839.2010.521526.

[26] WANG S C, AINDOW M, STARINK M J. Effect of self-accommodation on α/α boundary populations in pure titanium [J]. Acta Materialia, 2003, 51(9): 2485−2503. DOI: 10.1016/S1359-6454(03)00035-1.

[27] YANG J, WANG G, JIAO X, LI Y, LIU Q. High-temperature deformation behavior of the extruded Ti-22Al-25Nb alloy fabricated by powder metallurgy [J]. Materials Characterization, 2018, 137: 170−179. DOI: 10.1016/j.matchar.2018.01.019.

[28] YANG J, WANG G, JIAO X, LI X, YANG C. Hot deformation behavior and microstructural evolution of Ti-22Al-25Nb-1.0B alloy prepared by elemental powder metallurgy [J]. Journal of Alloys and Compounds, 2017, 695: 1038−1044. DOI: 10.1016/j.jallcom.2016.10.228.

[29] LI S F, KONDOH K, IMAI H, CHEN B, JIA L, UMEDA J, FU Y B. Strengthening behavior of in situ-synthesized (TiC–TiB)/Ti composites by powder metallurgy and hot extrusion [J]. Materials and Design, 2016, 95: 127−132. DOI: 10.1016/j.matdes.2016.01.092.

(Edited by ZHENG Yu-tong)

中文导读

2.6vol%TiBw/Ti6Al4V 复合材料热处理后微观组织定量分析及高温断裂机理研究

摘要：本文通过 1100 °C/1 h 真空热压烧结技术制备了 2.6vol%TiBw/Ti6Al4V 网状增强钛基复合材料，并建立了热处理参数与各相百分含量的量化关系。结果表明，在固溶温度 930~1100 °C 和时效温度 400~600 °C 之间，各相百分含量与固溶、时效温度呈线性变化。并且经过 950 °C/1 h 固溶处理与 600 °C/12 h 时效处理后，由于热处理过程中发生了静态再结晶，钛基复合材料呈现等轴状。对等轴钛基复合材料进行高温拉伸测试，结果表明，材料高温抗拉强度达到 772 MPa(400 °C), 658 MPa(500 °C), 392 MPa(600 °C) ,182 MPa(700 °C)，高温伸长率也分别为 9.1%(400 °C), 12.5%(500 °C), 28.6%(600 °C), 35.3%(700 °C)。通过对材料高温断口的分析，发现 TiB 晶须在 600 °C 温度以下能够起到很好的增强效果，但是当温度超过 700 °C 后，TiB 晶须与基体发生脱粘现象，导致 TiB 晶须的增强效果显著降低，并且使裂纹沿着晶界扩展。

关键词：钛基复合材料；热处理；力学性能；组织演变